

This work was written as part of one of the author's official duties as an Employee of the United States Government and is therefore a work of the United States Government. In accordance with 17 U.S.C. 105, no copyright protection is available for such works under U.S. Law.

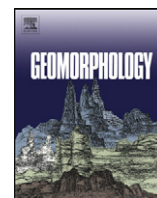
Public Domain Mark 1.0

<https://creativecommons.org/publicdomain/mark/1.0/>

Access to this work was provided by the University of Maryland, Baltimore County (UMBC) ScholarWorks@UMBC digital repository on the Maryland Shared Open Access (MD-SOAR) platform.

Please provide feedback

Please support the ScholarWorks@UMBC repository by emailing scholarworks-group@umbc.edu and telling us what having access to this work means to you and why it's important to you. Thank you.



Spatial and temporal analysis of a global landslide catalog



Dalia Kirschbaum^{a,*}, Thomas Stanley^{a,b}, Yaping Zhou^{a,c}

^a NASA Goddard Space Flight Center, Hydrological Sciences Laboratory, USA

^b Universities Space Research Association, USA

^c GEAR/Morgan State University, USA

ARTICLE INFO

Article history:

Received 14 July 2014

Received in revised form 9 March 2015

Accepted 10 March 2015

Available online 21 March 2015

Keywords:

Landslide catalog

TRMM

Extreme precipitation

Global analysis

Remote sensing

ABSTRACT

Landslide inventories are critical to support investigations of where and when landslides have happened and may occur in the future; however, there is surprisingly little information on the historical occurrence of landslides at the global scale. This paper presents a new publicly available global landslide catalog (GLC), which is based on media reports, online databases, and other sources. This database is currently available at <http://ojo-streamer.herokuapp.com/>. The 5741 points in the GLC provide a foundation for evaluating spatial and temporal trends in landslide activity from 2007 to 2013. Globally, landslides were reported most frequently from July to September. Most events occurred in Asia, North America and Southeast Asia. In contrast, fewer than 5% of the fatalities were reported in North America, suggesting a significant amount of under-reporting in other regions as well as potential discrepancies between developing and developed regions. Reported landslide events were also compared to satellite-based precipitation estimates from the Tropical Rainfall Measuring Mission (TRMM) to evaluate the co-occurrence of extreme precipitation and landslide activity. Of the 3550 points considered in a subset of the GLC, approximately 60% of the reported landslides have daily precipitation exceeding the 95th percentile of precipitation calculated over a 14-year TRMM record for the same location. This study also investigated how the recurrence interval of extreme precipitation corresponded to some of the most catastrophic landslide events. In spite of several reporting and cataloging biases, spatial and temporal analysis of the GLC suggests that it is a valuable database for characterizing global patterns of landslide occurrence and evaluating relationships with extreme precipitation at regional and global scales.

Published by Elsevier B.V.

1. Introduction

Some natural hazards, such as hurricanes or earthquakes, have comprehensive global monitoring networks, enabling scientists to compile the track statistics or focal mechanisms of these hazards with a high degree of accuracy. In contrast, identifying where and when landslides occur has proven difficult due to their limited spatial extent and lack of consistent reporting networks. This paper presents the global landslide catalog (GLC), an online database of rainfall-triggered landslides from 2007 to the present. The GLC provides a new opportunity to examine patterns of landslide activity at multiple spatiotemporal scales. This catalog can be accessed at: <http://ojo-streamer.herokuapp.com/>.

Traditionally, landslide inventories have been compiled in several different ways. Some inventories are presented as point-based or polygon-based maps highlighting historical landslides over local or regional scales. These studies use aerial photographs or other remotely sensed products to identify landslide scarps within the temporal window of the available photographs or imagery (Booth et al., 2009;

Guzzetti et al., 2012). A second type of inventory focuses on a single, often catastrophic, triggering event and uses airborne or satellite imagery together with ground-based surveys to characterize the extent, area and volume of triggered slope failures (Bucknam et al., 2001; Xu et al., 2013; Murillo-García et al., 2014). Both of these inventory types are fundamental to the comprehensive assessment of landslide susceptibility, vulnerability and risk for a specific area. Lastly, other landslide inventories compile information from a combination of newspaper reports, published articles, aerial photographs and other sources, typically as point-based databases (Guzzetti et al., 1994; Pradhan, 2010). The GLC uses the third approach to catalog global rainfall-triggered landslide occurrences.

There have been a few attempts to characterize landslides at the global scale, usually focusing on a specific type of event, triggering mechanism or impact. Petley (2012) has compiled a global database of fatal landslides based on media reports, online databases, personal communications and other sources. With this inventory he has been able to characterize global patterns in loss of life from landslides resulting from all triggers, relating these patterns to seasonal variations in peak rainfall and proximity to population centers (Petley et al., 2005; Petley, 2012). The EM-DAT International Disaster Database compiles information on all types of disasters but limits its reporting to events which have killed

* Corresponding author at: 8800 Greenbelt Road, Code 617, Greenbelt, Maryland 20771, USA. Tel.: +1 301 614 5810, fax: +1 301 614 5808.

E-mail address: dalia.b.kirschbaum@nasa.gov (D. Kirschbaum).

10 or more people, affected 100 or more people, or resulted in a declaration of a state of emergency or call for international assistance (Guha-Sapir et al., 2014). While major landslide events are often captured, the EM-DAT database of landslides (cataloged as wet or dry mass movements) is quite limited due to the practice of attributing landslide impacts to other hazards such as floods or tropical cyclones. Lastly, other efforts to enable citizen reporting of landslides (e.g. <http://landslides.usgs.gov/dysi/form.php>, <https://www.bgs.ac.uk/landslides/report.html>) can potentially characterize landslides missed by traditional surveys; however, the databases are usually limited to the country in which the program is being hosted. The GLC considers all types of mass movements triggered by rainfall, referenced herein as landslides, which have been reported in the media, disaster databases, scientific reports, or other sources. This research updates the methodology and analysis presented in (Kirschbaum et al., 2010), expanding the analysis to include seven full years of data. This research also utilizes a near-global satellite-based precipitation record to identify patterns in extreme daily or multi-day rainfall associated with the landslide reports.

This paper first introduces the methodology and attributes of the GLC. Next, the seven years of available data are evaluated based on spatial, temporal and socio-economic variables. The paper then considers the extent to which extreme rainfall corresponds to reported landslide activity, considering both global and regional examples. The paper concludes by discussing how the results of the GLC may be improved and applied.

2. Methods

2.1. Data collection

The GLC was developed with the goal of identifying rainfall-triggered landslide events around the world, regardless of size, impacts or location. The catalog is compiled from a variety of sources, including online media reports, disaster databases, scientific reports, blog entries, personal communication and other sources. Online news articles serve as the primary sources of information for the landslide catalog and are found using Google Alerts (www.google.com/alerts) and other search engine options. When possible, multiple sources are consulted for redundancy. The current GLC contains 5741 reports from the years 2007–2013. Each reported landslide event is characterized by 16 unique fields, which are summarized in Table 1.

For analysis purposes, it is often helpful to separate small, shallow (i.e. less than a few meters deep) slope failures with short runouts from large to catastrophic landslides that cover broad areas. We redefine a qualitative landslide size metric based on the table presented in Kirschbaum et al. (2010) to categorize each report as a small, medium, large or very large landslide (Table 1).

2.2. GLC uncertainty

There are many challenges in characterizing landslide events from news reports and other text-based sources. Information can vary widely in terms of both accuracy and availability, resulting in several biases and uncertainties that affect the GLC. Sometimes the problem is simply one of omission. Most landslide reports are obtained from English-language media. As a result, large numbers of landslides were recorded in the United States and the United Kingdom, relative to other locations. Searches have been attempted in Spanish, Portuguese, Vietnamese and other languages with limited success. We have also observed biases resulting from political or economic differences among regions. In some large areas characterized by steep topography and abundant rainfall, few landslides have been reported when many more would be expected from the underlying geomorphology. Information on landslide impacts may also be inflated or minimized in some cases. Because the database was compiled over multiple years, improved access to information has probably affected the accuracy and completeness of the GLC. While we

Table 1

Summary of fields included in the GLC. *Landslide type classifications are modified from Cruden and Varnes (1996) and the USGS (2004).

Category	Information on category
ID	Unique ID for each reported landslide event
Date	Reported year, month and day of the landslide event, (not when it was reported). Separate columns for year, month and day.
Time	Reported hour and minute of the failure, recorded as HH:MM (24 clock, local time). This field may also include an approximate time of day if known (e.g. morning, afternoon, evening).
Location	Latitude and longitude of the reported event
Country	Country in which the landslide occurred
Nearest place	Additional location information, including the nearest geographic location (e.g. village, city, region, landmark) if known.
Landslide type	Mass movement types are included if known or specified in the source and includes the most frequently reported types of events*: landslide, mudslide, debris flow, rockfall, earthflow, translational slide, snow avalanche, lahar, complex event, riverbank collapse, creep, other or unknown.
Landslide trigger	Includes the most common triggers of landslide events (more than one trigger can be specified). These include: rain, downpour, continuous rain, tropical cyclone, monsoon, mining or digging, construction, earthquake, flooding, volcanic eruption, freeze/thaw, snowfall/snowmelt, or unknown.
Storm name	Includes the name or number of a tropical cyclone if identified (e.g. Hurricane Sandy, Typhoon Etai, Tropical Depression No. 12)
Fatalities	Number of reported fatalities in the event
Other impacts	Number of people injured, affected or houses/buildings affected in the event
Information source	Source of report information, includes news source, field observation, disaster database, personal communication, etc.
Information link	URL link to news report or other online source that has a listing of the report.
Comments	Includes event information such as dimensions of the landslide, characteristics, impacts, timing or situation resulting in the slope failure and other relevant information.
Location accuracy	This field assigns a qualitative uncertainty in the landslide location based on the estimated area over which the landslide realistically occurred, described as a radius from the event coordinates to a given radius (in kilometers). <ul style="list-style-type: none"> • Location known exactly or within 0.1 km • Event location known within 1 km • Event location known within 5 km • Event location known within 10 km • Event location known within 15 km • Event location known within 25 km • Event location known within 50 km • Event > 50 km • Unknown
Landslide size	This category is to identify the relative size of the landslide in an attempt to differentiate small landslides occurring in backyards and along roads from larger landslides that have caused catastrophic damage and cover wide areas. The "Size Classification" values are from Kirschbaum et al. (2010), which describe the landslide cataloging methodology. We have mapped these 1–5 rankings into the following categories: <ul style="list-style-type: none"> • <i>Small</i>: Small landslide affecting one hillslope or small area (Formerly Size Class 1): Minimal impacts to infrastructure and roads, no fatalities. • <i>Medium</i>: Moderately sized landslide that could be either a single event or multiple landslides within an area, and involves a large volume of material (Formerly Size Classes 2 and 3): Moderate impact to infrastructure and roads, may result in fatalities. • <i>Large</i>: Large landslide or series of landslides that occur in one general area but cover a wide area: Substantial impacts to infrastructure and roads, likely moderate to high number of fatalities • <i>Very Large</i>: Very large landslide or multiple events that affect an entire region (often encompassing an entire village or larger area): Catastrophic impacts to infrastructure and roads, high numbers of fatalities.

do not observe a continuously increasing (or decreasing) annual number of reports for any country with more than 10 total entries in the database from 2007–2013, changing availability to internet access and evolving policies on media reporting for some countries, such as

China, may have affected the spatial and temporal reporting accuracy over time.

A second form of bias results from the difficulty of describing specific landslides from the general description provided by a typical media report. Landslide events and impacts are often grouped with or attributed to other hazards such as tropical cyclones and flooding. Therefore, it can be very challenging to determine the location of each individual landslide event as well as any directly related fatalities or impacts (e.g. “Typhoon Morakot caused flooding and landslides in Taiwan”). In these cases, multiple sources are considered if available. However, when very little information is given, the event is not included in the catalog. In addition, if a significant rainfall event triggered multiple landslides over an area, the actual number of entries in the GLC can vary based on the availability of information for each individual landslide. As a result, the GLC may underemphasize the impact of major storms that generate significant numbers of landslides.

Increased media coverage near populated areas may be another source of bias. Landslides are more likely to be reported in areas where they affect people (i.e. along roads or within populated areas). In addition, the initiation zone of the landslide is usually impossible to locate from media reports since the events tend to be reported near a village or town or along a road between two towns. If damages occur in a landslide’s runout path, media reports often identify the location of the impacts, rather than the initiation point. As a result, we define a

“landslide location accuracy” field to differentiate reports where the landslide is well identified (e.g., intersection of two clearly defined roads), from reports where only a broad area is given (e.g., Gansu Province, China). A radius (in km) is specified for each latitude–longitude pair that indicates the maximum distance from the given point where the landslide is likely to have occurred. Due to the challenge of accurately identifying the initiation points of landslides, topographic characteristics associated with GLC reports tend to underestimate the slope at which failure occurs.

The biases and uncertainties inherent in this cataloging method have been documented by other studies (Guzzetti, 2000; Petley et al., 2005; Kirschbaum et al., 2010). Despite these problems, the GLC provides a minimum number of rainfall-triggered landslides occurring at the global scale.

For portions of the GLC analysis we select a subset of GLC reports (herein GLC subset) that have the most accurate information on location, trigger and size. The GLC subset contains 3550 points distributed around the world. Landslides were included in the GLC subset if the following conditions were met: 1) the location accuracy was better than 25 km; 2) the landslide trigger was identified as rainfall; 3) the landslide occurred between 50°N and 50°S latitude (relevant for the precipitation analysis); and 4) the landslides were characterized as being of medium size or larger. Some landslide points were also removed if a large number of landslides were reported within the same area for the same event

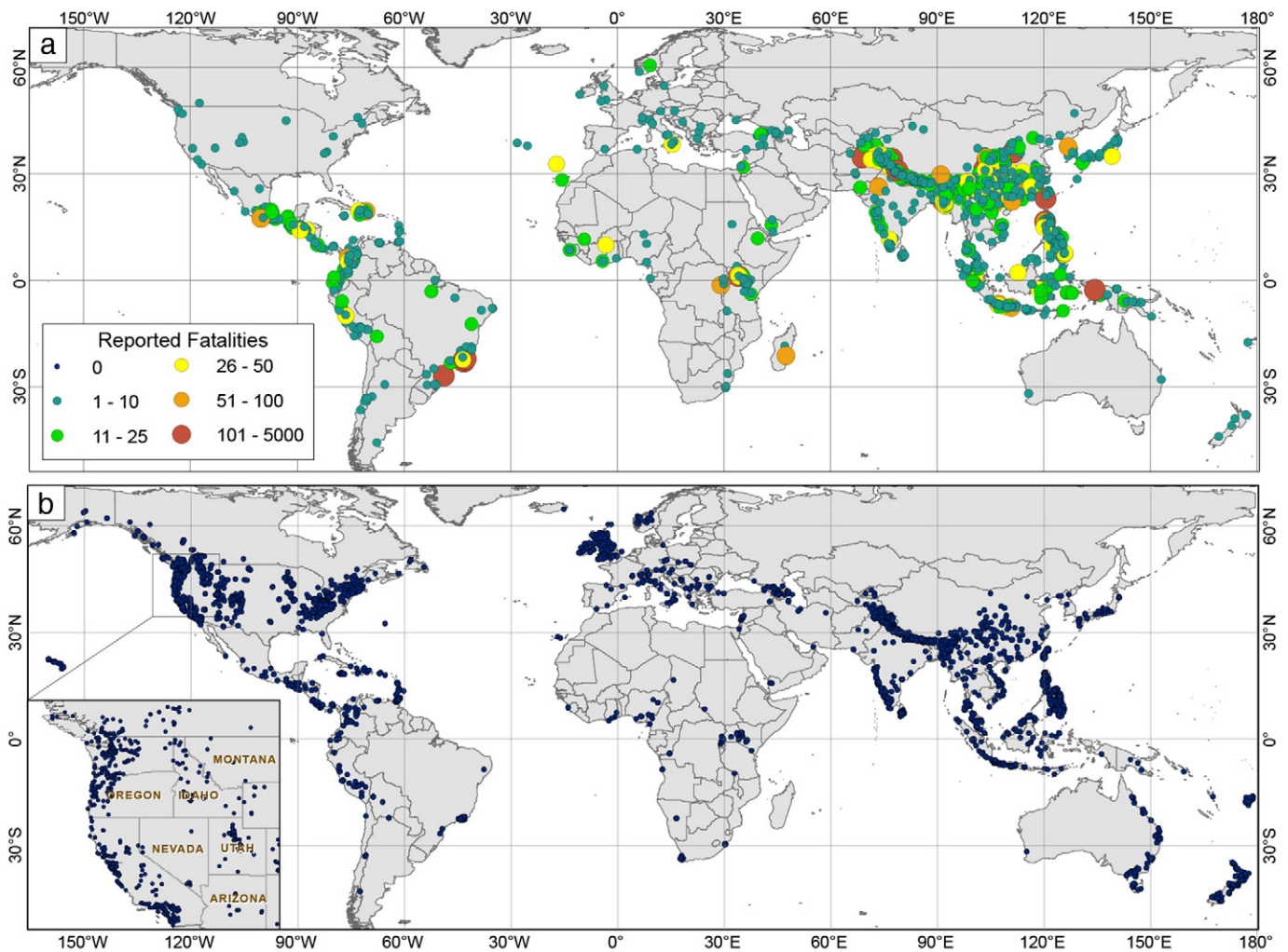


Fig. 1. Global map of reported landslide events from 2007–2013 in the GLC showing a) landslides with fatalities and b) landslides with no fatalities. The size and color of the data point indicates the number of reported fatalities for each event. A subset from the U.S. west coast is shown to highlight the distribution of landslide reports with no fatalities in this area.

due to unusually good reporting (e.g. a rainfall event that triggered numerous smaller landslides in Rio de Janeiro, Brazil in April 2010), which can serve to overemphasize a particular event or region in the statistics. The GLC subset is used to evaluate relationships with population density, road networks and rainfall.

2.3. Rainfall analyses

Studies on rainfall intensity and duration are typically conducted over local, country or regional scales where there are sufficient in situ gauges (e.g. Larsen and Simon, 1993; Crozier, 1999; Frattini et al., 2009; Meyer et al., 2012). A smaller pool of research has used a collection of global landslide points or regionally defined rainfall intensity–duration (ID) thresholds to estimate rainfall triggering relationships at the global scale (e.g. Caine, 1980; Hong et al., 2006; Guzzetti et al., 2008; Kirschbaum et al., 2012). ID thresholds specify the estimated boundary above which intense and/or prolonged rainfall is expected to trigger a landslide. While these empirically derived curves have proved useful in local or regional settings, Guzzetti et al. (2008) and Kirschbaum et al. (2009) identified the need for regionally varying thresholds and alternative ways for characterizing extreme landslide-triggering rainfall at the global scale.

Satellite-based precipitation data provides an opportunity to examine the spatial and temporal patterns in landslide-triggering rainfall over broader areas. This study uses a satellite-based record of precipitation from the Tropical Rainfall Measuring Mission (TRMM) Multi-satellite Precipitation Analysis (TMPA) Version 7 Real-time product, which is available from 50°N to 50°S at a $0.25^\circ \times 0.25^\circ$, 3-hourly resolution from 2000–2013 (3B42RT) (Huffman et al., 2007, 2010). The TMPA algorithm first uses the TRMM Microwave Imager (TMI) observations to adjust passive microwave estimates from other satellite sensors. Next, infrared data from sensors on the international constellation of geosynchronous-orbit meteorological satellites are collectively calibrated to be consistent with the microwave estimates with time- and space-varying coefficients. These calibrated infrared and microwave data are then merged by taking imager, sounder, or calibrated IR where available. The final product has quasi-global coverage (50°N–S), though it can be less accurate outside the 35°N–S coverage zone of the TRMM instrument itself against which data from other sensors is adjusted or calibrated.

We consider “extreme rainfall” to be daily to multi-day rainfall accumulations at the upper limits of the precipitation distribution. This research extracts TMPA RT precipitation information for the GLC subset points at the corresponding pixel and evaluates how the rainfall observed for each reported landslide compares to rainfall distributions recorded over the 14-year satellite-based record. The real-time version of TMPA V7 was used so that results from this analysis may be applied to future real-time rainfall-triggering threshold estimations. Two different methods are applied to define extreme rainfall: percentiles and average recurrence intervals (ARIs).

The percentile-based approach first calculates the maximum 1-day, 3-day, and 7-day rainfall within a two week window surrounding each reported landslide event date (3 week window for 7-day accumulations). Rainfall percentiles (50th, 75th, 95th and 99th) are then computed for each of the landslide points based on the 14-year rainfall time series with non-rainfall days removed. Lastly, the maximum rainfall for the 1, 3, and 7 day accumulations are compared to the corresponding percentiles to determine if the maximum rainfall associated with the landslide reports exceeded the calculated percentile values.

Extreme rainfall can also be evaluated according to the probability of occurrence of the rainfall accumulation over a specified duration for a given year. Return period or average recurrence interval (ARI) has been used in the hydrological community to depict the rarity of flood events for decades. An event with an ARI of 20 years means the probability of occurrence in any given year is 1 in 20 or 5%. ARI is computed from frequency analysis of historical precipitation data by fitting the

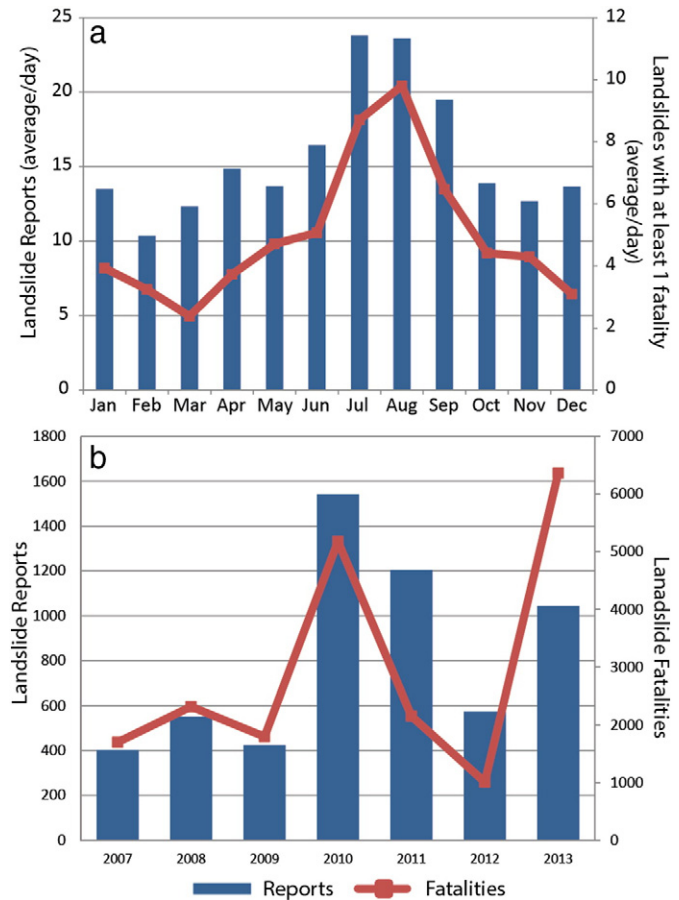


Fig. 2. Distribution of GLC database for a) reports and events with at least 1 fatality by month (shown as average number of reports per day); and b) reports and total landslide fatalities by year from 2007–2013. The peak of landslide fatalities in 2013 primarily corresponds to the event in Kedarnath, India which killed approximately 5000 people.

data to a 3-parameter generalized extreme value (GEV) distribution function (Bonnin et al., 2003).

To calculate the ARI, the annual maximum (AM) precipitation accumulations are first computed from running totals of 1, 2, 3, 5, 7 and 10-day time series from TMPA RT data for each year and for each grid box. Then, the 3-parameter GEV distributions are derived by fitting the AM series using open source MatLab GEV software.¹ From derived GEV statistical parameters, lookup tables for different ARI values from 2 to 100 years are generated for rain accumulations of 1 to 10 days for each grid point. Finally, for a specific rain accumulation at a given grid point, the rain amount is converted to ARI with the right lookup table by simple interpolation (Zhou et al., in press). We have computed 1 to 10-day rain accumulations prior to the date of the landslide and the corresponding ARIs for a $5^\circ \times 5^\circ$ box centered on the landslide location for each of the 3550 landslides in the GLC subset. The relationship between extreme rainfall and landslides using both methodologies are presented in Section 3.2.

3. Results

3.1. GLC reports and fatalities

The entire GLC contains 5741 reports in the years 2007–2013, representing 124 countries and territories. There are over 20,500 fatalities reported in this database from 1827 events (~30% of the total

¹ <http://www.mathworks.com/help/toolbox/stats/gevfit.html>.

reported events). Fig. 1 displays a global map of the GLC, highlighting many “hotspot” landslide areas. The map also shows clear distinctions between landslide reports with few or no fatalities compared to reports with many fatality estimates. The United States, United Kingdom, Australia and New Zealand contain a large number of reported landslides but few fatalities. These four countries account for 27.5% of landslide reports but only 0.7% of the landslide fatalities and 1.6% of the landslides that have caused at least 1 fatality. In these areas, smaller landslides are much better identified due to the accessibility, transparency and abundance of English language speaking media relative to other areas.

Fig. 2a displays the monthly GLC reports and landslides with at least one reported fatality, shown as the average number of events per day according to month. Landslide reports and landslides with reported fatalities peak during the Northern Hemisphere summer (July through

September), corresponding to the Southwest, South, and East Asian monsoon seasons and the Northern Hemisphere tropical cyclone peaks. This global pattern has been corroborated by previous studies (Petley et al., 2005; Petley, 2012). There is also a secondary peak in December and January resulting primarily from landslides in South America, particularly Brazil, Colombia and Peru as well as Indonesia and Malaysia.

Yearly differences in landslide reports and total fatalities are shown in Fig. 2b. The graph highlights a peak in events and fatalities in 2010, as well as secondary peaks in 2011 and 2013. The peak in fatalities in 2013 is due to one devastating event in Kedarnath, India on June 16th, 2013 that killed an estimated 5000 people (EM-DAT, 2014). If that data point were removed, the total number of fatalities would be approximately 1364 and rank as one of the lowest annual totals in the GLC. However, the number of landslide events that caused at least 1 fatality

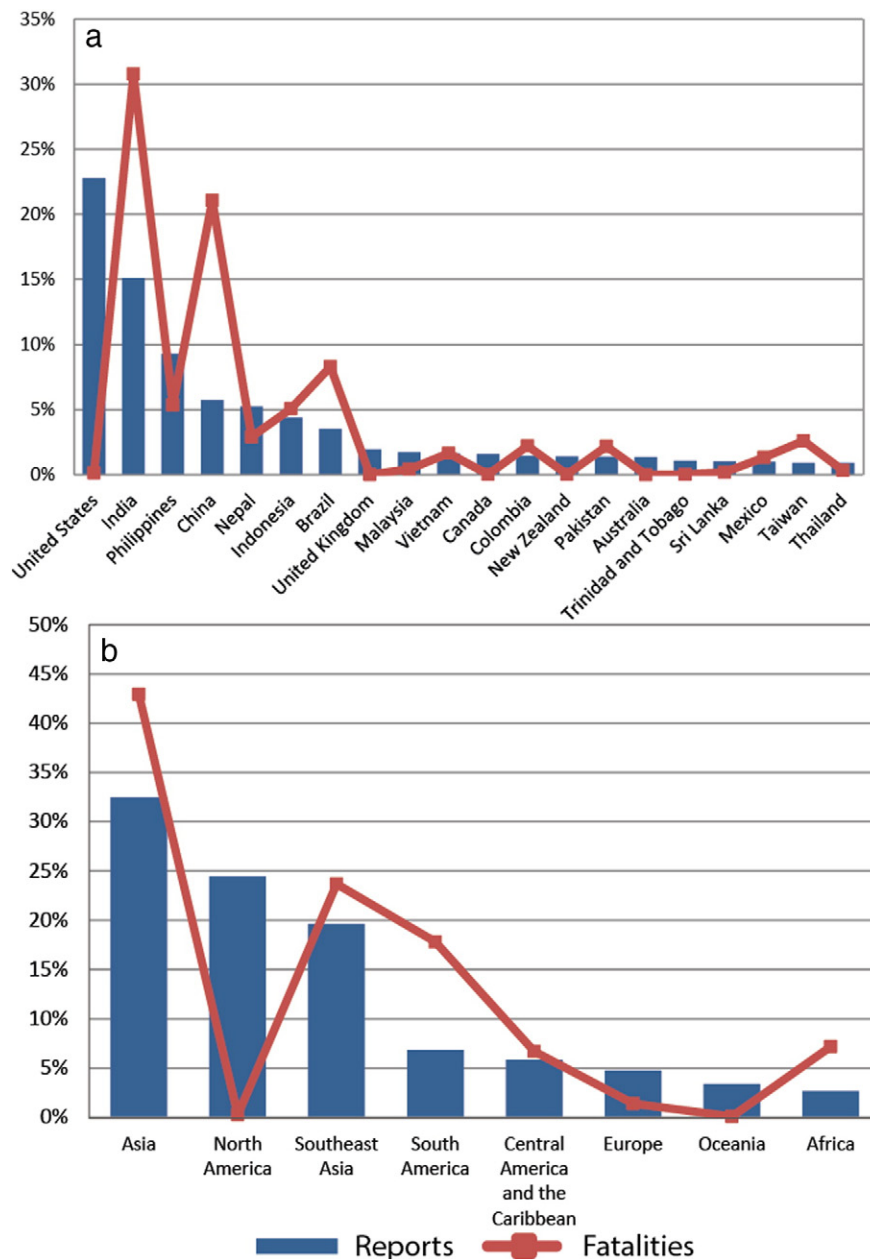


Fig. 3. Landslide reports (blue) and landslide fatality estimates (red) for all years in the GLC as a function of a) country (top 20 countries with the most reports); and b) region. The two most deadly landslides in Zhouqu, China in 2010 and Kedarnath, India in 2013, were removed because these two events account for 33% of all fatalities reported from 2007–2013.

in 2013 is actually the highest of all years (544 events). The variability of reports and fatalities over the seven years of the database is likely the result of multiple factors. We have observed active El Niño Southern Oscillation (ENSO) cycles in 2010, which may have increased extreme precipitation events in some regions and, consequently, the number of landslides (Kirschbaum et al., 2012). Other factors, including subtle changes to the cataloging methodology and the time of report acquisition, might have affected the statistics but are not expected to have a significant impact. There is no statistically significant trend in fatalities or landslide reports, probably due to the relatively short time span of the GLC, though major events also tend to bias the catalog.

Results from the 7-year record are also shown by country (Fig. 3a) and region (Fig. 3b). The United States has the highest number of reported landslides in the database (1308) but only 30 reported fatalities from 2007–2013. Comparatively, the Oso, Washington landslide which took place on March 22nd, 2014 had 42 confirmed fatalities and ranks as the most devastating landslide in the United States within the past decade (Berman, 2014; Snohomish, 2014). This underscores how a single event can significantly impact the GLC statistics. India, the Philippines, China, Nepal and Indonesia consistently have the highest number of reports in the record. In Fig. 3b, Asia and Southeast Asia are ranked first and third in the number of reports and first and second in the number of landslide fatalities, respectively. The large number of fatalities in Brazil is due to a major event that occurred outside of Rio de Janeiro in January 2011, where landslides caused over 900 fatalities (referred to herein as Brazil 2011 landslides).

3.2. Socio-economic indicators

3.2.1. GDP per capita

In addition to observing the spatiotemporal patterns of the GLC, reports from each country were compared with the corresponding 2012 GDP per capita (2012 USD; World Bank, 2014) to evaluate the relationship between the country's level of development, reported events and fatalities. Only countries with more than 20 events recorded in the GLC are included in this analysis. Fig. 4a illustrates the relationship between GDP per capita and the percentage of landslides within each country that had reported fatalities. There is an exponential decrease in GDP per capita as the percentage of landslides with fatalities increases. The exceptions to this trend are Italy (33% of reports with fatalities) and Japan (52% of reports with fatalities). Due to the primary languages of two countries, reports are probably biased toward large events and miss smaller events that have few impacts or fatalities. Fig. 4b highlights the relationship between GDP per capita and total reported landslide fatalities for the GLC evaluation period. The richest countries suffered the fewest fatalities, while hundreds died in many of the world's poor countries.

3.2.2. Population and road networks

In order to look at the relationship between population and landslide occurrence, the GLC subset was used to look at reports with a location accuracy better than 5 km and 25 km. The reports were evaluated separately against a population density dataset from LandScan, which catalogs ambient global population at a 1 km resolution (30" × 30") (Bright et al., 2012). Circular buffers were calculated in ArcGIS (ESRI, 2011) around each landslide corresponding to the location confidence (5 or 25 km) and the maximum population value within that area was extracted. To evaluate how population near reported landslides compares with the global population distribution, an equal number of random points were generated using ESRI's "Create Random Points" geoprocessing tool for the LandScan data extent (i.e. no points at sea) between 50°N and 50°S. Results for the population comparison between landslide and non-landslide areas within 5 km and 25 km buffers are shown in Fig. 5a and b.

Previous studies have observed the contribution of roads to landslide initiation (Haigh et al., 1995; Larsen and Parks, 1997; Petley

et al., 2007). Here we evaluate the total length of road networks within the same 5-km or 25-km buffer zones introduced above using the Vector Map Level 0 road database (Vmap0, 2009). Landslides and randomly generated points were compared and are shown in Fig. 5c and d. Both graphs indicate that there are longer road networks within the landslide point buffer areas, although the difference is more pronounced for the 5-km buffer zones. These differences suggest that landslides are more likely to be reported in areas with higher populations and with denser road networks; however, it does not follow that more landslides occur overall. The declining frequency of landslides in areas with the densest road networks may be due to the fact that dense road networks are rarely constructed in mountainous terrain. The proportion of the difference between distributions is difficult to determine. This pattern may also indicate the role of human activity in initiating slope failures.

Characterizing biases due to reporting is an ongoing challenge with databases compiled from media reports. Fig. 5 suggests that the reported landslides and randomly selected points for population and road networks have moderate differences in road networks and more pronounced differences in population. Simple correlation analysis from the datasets indicate that the landslide and non-landslide datasets for road networks have a higher correlation coefficients (0.82 for 5-km and 0.57 for 25-km buffer areas, respectively), whereas results for population show much weaker relationships with landslide and non-landslide points with correlation coefficients of 0.18 and 0.09 for 5 and 25 km buffers respectively.

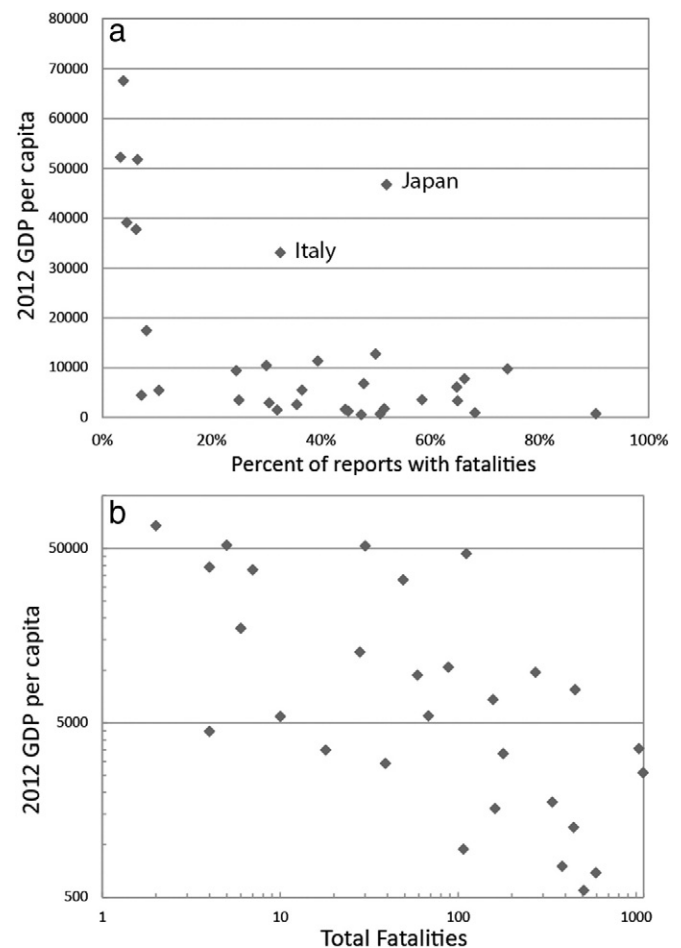


Fig. 4. Evaluation of countries with at least 20 landslide reports over 2007–2013, showing the country's 2012 GDP per capita (2012 USD) versus: a) the percentage of landslide reports with at least one fatality; and b) the total number of fatalities for each country within a log–log plot.

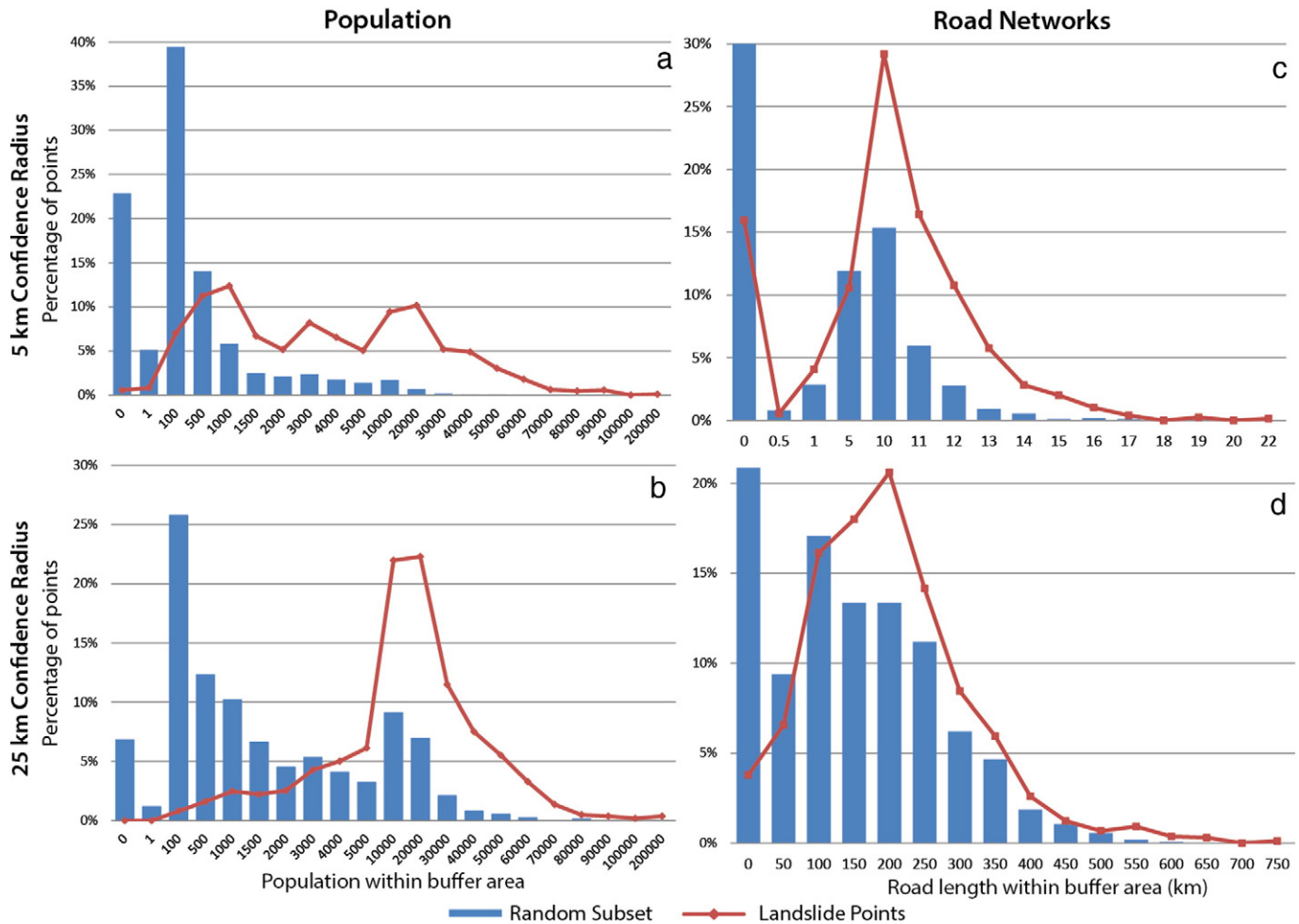


Fig. 5. Subsetted group of the GLC (red line) versus an equal number of randomly selected points (blue bars). Correlation coefficients (cc) were calculated for each figure comparing the random subset to landslide points. Population was evaluated for GLC points known within a) 5 km ($cc = 0.18$) and b) 25 km ($cc = 0.08$) and plotted based on the maximum population within each buffer area, shown as the percentage of points within each bin. The length of road networks (km) were extracted for the same GLC and randomly selected points for c) 5-km ($cc = 0.82$) and d) 25-km ($cc = 0.57$) buffer areas.

3.3. GLC and extreme rainfall

3.3.1. Percentile evaluation

The TMPA time series was extracted at each GLC subset point and aggregated from a 3-hourly time series to a daily accumulation. Fig. 6 compares the global distribution for the maximum daily precipitation at the landslide locations (red) with the 90th (light blue), 95th (dark blue) and 99th (green) percentiles for the same locations over the 14-year TRMM record based on the number of reports. Fig. 7 presents the same daily distributions but divided into eight geographic regions. Correlation coefficients were calculated for the distributions of the maximum daily rainfall and 90th, 95th and 99th percentiles at the global and regional level. The global distribution of the GLC subset has the best correlation with the 95th percentile of rainfall. Regional plots show a large range of rainfall values, with large daily rainfall values over Asia, Central America and Southeast Asia. Overall, the 95th percentile exhibited the strongest relationship with landslide triggering rainfall at the regional level. Landslide points in Oceania were associated most closely with the 90th percentile distribution, while the relationship was weak in Europe, likely due to the small sample size. While there is still large variability in the distributions, there is a clear positive skewness toward higher precipitation values for all of the regions considered.

The rainfall observed at each landslide event was directly compared to the historical rainfall accumulated over 1, 3, and 7-days. The proportion of points exceeding the percentile for the same pixel is shown in

Table 2. 78% of the GLC subset points exceeded the 90th percentile values for the 1-day rainfall, with the percentage of points decreasing from 75% to 73% for the 3 and 7-day accumulations, respectively. Points exceeding the 95th percentile have less of a range (61% to 56% of the database) from 1 to 7-day accumulations. Lastly, the 99th percentile has the smallest spread with approximately 26–27% of the GLC points exceeding the threshold. 291 landslide events had daily maximum rainfall of less than 10 mm, suggesting that the location was misreported, rainfall was not the dominant trigger of the event, or the satellite rainfall underestimated the peak intensities for that event. If these points are removed, approximately 30% of the GLC subset points exceed the 99th percentile of rainfall for all accumulation windows.

Fig. 8 compares the distribution of precipitation extremes calculated from the GLC subset points to global ID thresholds published in previous literature (Caine, 1980; Crosta and Frattini, 2001; Hong et al., 2006; Guzzetti et al., 2008). The ID threshold developed by Hong et al. (2006) was derived from TMPA data using a small selection of significant landslide events globally. The threshold by Caine (1980) was also calculated using larger landslide events, which may have been triggered by greater rainfall intensities and durations compared to many of the landslides in the GLC. The Guzzetti et al. (2008) threshold was compiled from a large number of regionally focused ID thresholds. The box plots show 1, 3, and 7-day rainfall accumulations according to the quartile distributions compared to the ID threshold. The spread of the ID thresholds around the GLC precipitation values suggests that three of the four

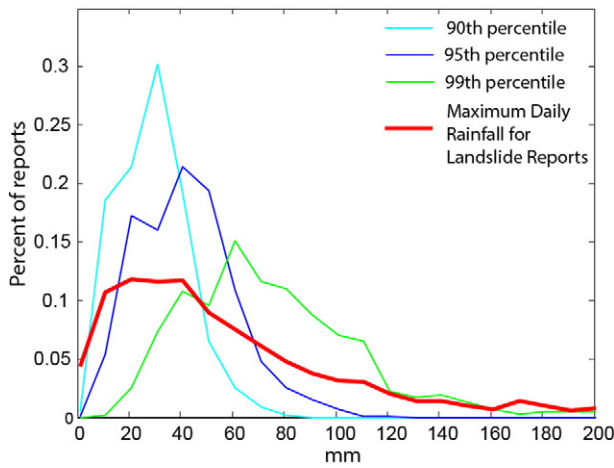


Fig. 6. Percentage of all GLC subset points for daily rainfall accumulations (mm) showing the 90th percentile (light blue), 95th percentile (dark blue), 99th percentile (green) and maximum daily rainfall at the landslide date (red).

rainfall thresholds are well within the range of the GLC-based extreme rainfall values. Results indicate that the GLC may be a useful catalog to further investigate rainfall ID relationships both regionally and globally. However, a truly robust ID evaluation would require substantially better spatiotemporal accuracy and many more landslide points to account for regional heterogeneities in surface type, precipitation regime, etc. The comparison presented here suggests that the GLC may be used in concert with other inventories to better understand rainfall intensity and duration at a regional scale.

3.3.2. Rainfall average recurrence intervals

TPMA RT rainfall was also evaluated for average recurrence intervals within a $5 \times 5^\circ$ box surrounding the landslide locations in the GLC subset. The results in Table 3 indicate that between 53.8 and 81.6% of the reported landslides occur in the vicinity of heavy precipitation, with a greater than 1-year return interval depending on the accumulation window considered. For each of the ARI values (1, 2, 5, and 10-years), the number of GLC events with longer ARIs increases as the accumulation window increases from 1 to 10 days. However, for each accumulation window, the percentage of GLC events decreases as the ARI increases. The results in Table 3 also show that as the ARI gets larger, the percentage of GLC events exceeding the ARI becomes smaller. For example,

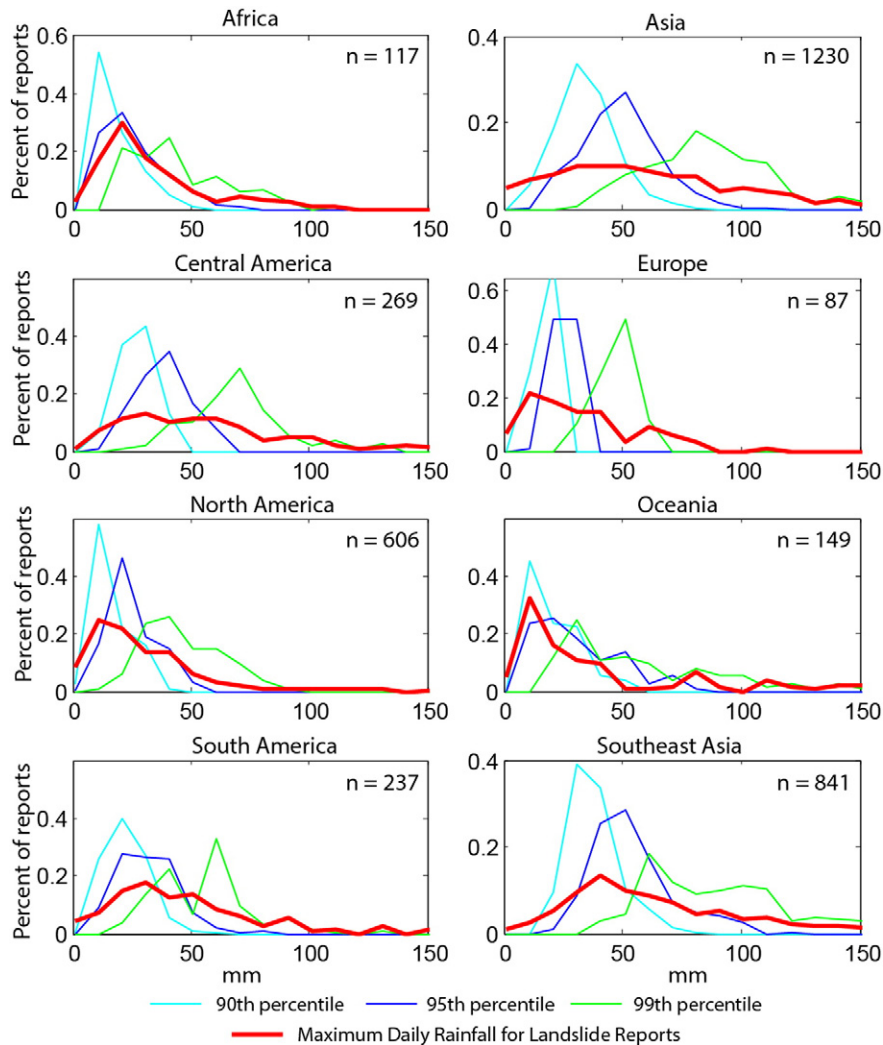


Fig. 7. Rainfall signatures of landslide events and corresponding percentiles by region for 1-day accumulations. Graphs show the percentage of reports for the 90th percentile (light blue), 95th percentile (dark blue), 99th percentile (green) and maximum daily rainfall at the landslide date (red). For this analysis, 14 points were not included because the date of the event was too close to the end of the available rainfall record. The total sample size for each region is included in the top right corner of each graph.

Table 2

Percentage of landslides exceeding the 50th, 90th, 95th and 99th percentiles based on 1, 3 and 7-day rainfall accumulations within the several weeks surrounding the reported event.

	50th	90th	95th	99th
1-day	97.4%	78.1%	61.3%	27.3%
3-day	96.5%	74.7%	59.5%	27.5%
7-day	96.9%	72.5%	56.3%	25.9%

approximately 54 to 82% of the points have an ARI ≤ 1 year compared to a spread of 22 and 31% with an ARI of ≥ 10 years as the rainfall accumulation changes from 1 to 10 days. This suggests that the percentage of rainfall events with the most extreme rainfall (ARI ≥ 10) may be somewhat independent of the accumulation considered.

When comparing the percentile results in Table 2 to ARI results in Table 3, we see similar patterns in that lower percentile values (50th and 75th) and shorter ARI (1–2 years) have a higher percentage of reports. Results differ between the two tables where the percentage of GLC points exceeding each ARI category for 1 to 10 days increases with longer accumulation windows, which is opposite from what is presented in Table 2. This pattern can be explained by the different but complementary characteristics of each method. First, the ARI describes the maximum average recurrence interval of any cell within the $5 \times 5^\circ$ box, regardless of its proximity to the landslide location. The maximum precipitation event could be as far as 250 km from the landslide location and part of a different storm system entirely. In addition, the ARIs are evaluated as accumulations ending on the date of the reported landslide event. Consequently, if the GLC reported date (in local time) differs from the actual time of the initiation, or if the landslide was triggered after the major rainfall event, the ARI may not necessarily be capturing the rainfall signatures associated with the landslide-triggering event itself. The percentile calculations apply a moving window around the date of the landslide to account for this uncertainty and may be able to better resolve short duration (1-day) events. If the reported landslide location has a large confidence radius, then the rainfall considered may not be immediately responsible for the reported landslide. Future studies could consider rainfall in a flexible space and time window to capture some of the uncertainty associated with landslide dates to better resolve possible landslide triggering events. However, this approach may sacrifice the precision of the technique and therefore should ideally be evaluated in a continuous, real-time context if it were to be considered as an input within a real-time hazard system.

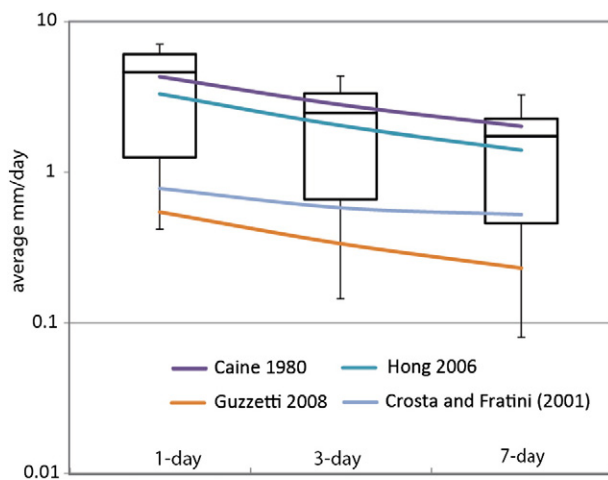


Fig. 8. Comparison of maximum accumulations for 1, 3, and 7-days for the subsetted GLC archive represented as box plots with the mean, upper and lower quartile with maximum and minimum values. Results are compared with four global intensity–duration thresholds: Caine, 1980; Hong et al., 2006; Guzzetti et al., 2008; Crosta and Frattini, 2001.

Table 3

Percentage of landslide points within an average recurrence interval (in years) greater than or equal to 1, 2, 5 or 10 years based on rainfall accumulations from 1 to 10 days within a $5 \times 5^\circ$ area surrounding the reported landslide event.

		Average recurrence interval			
		≥ 1	≥ 2	≥ 5	≥ 10
Rainfall accumulation window	1-day	53.8	43.5	29.8	22.0
	2-day	63.2	53.5	33.6	24.6
	3-day	67.7	57.6	37.2	25.4
	5-day	75.1	61.7	38.6	26.7
	7-day	77.7	66.0	40.6	28.6
	10-day	81.6	69.0	44.2	31.3

3.3.3. Extreme landslide events

Analysis of the GLC indicates the key role of major landslide events in driving high fatality estimates for specific years and regions. We investigate five catastrophic landslide cases over the 2007–2013 record in order to determine whether extreme rainfall clearly contributed to the landslides. The cases span multiple continents, trigger types and numbers of fatalities. Table 4 shows the ARI from 1 to 10 days, the maximum ARI (in years) and the 1, 3, and 7-day ARIs for each case. The maximum rain is also extracted for each of these events at 1, 3, and 7-day accumulation windows corresponding to the maximum rainfall within a 2 to 3 week window surrounding the event.

Fig. 9 highlights the 5 case studies outlined in Table 4 and shows the ARI for 1, 3 and 7-days within a $5 \times 5^\circ$ box centered on the landslide report, shown as the black triangle. The ARI is calculated within each window and results for the most intense precipitation (highest ARI in years) are shown in shades of red to purple. For some of the events, the maximum ARI within all the accumulation windows coincides with the landslide report; however, for some of the events (Case 2 and Case 5) peak rainfall is observed elsewhere in the region. For four of the five cases, ARIs greater than 50 years were estimated within the vicinity of the landslide location in at least one accumulation window, which emphasizes the necessity of using multiple accumulation windows to capture heavy rain events in varying durations.

Case 5 from Zhouqu, China showed less pronounced results because this was a short-duration (less than 1 h), high-intensity event that took place in the mountains above the city of Zhouqu. This peak rainfall intensity and previous wet weather resulted in a buildup of water and debris that blocked a small river north of Zhouqu, eventually leading to a dam breach which swept down and into the town. Deforestation and illegal mining were also reported to have increased susceptibility in the area (Oster and McMahon, 2010). Due to the short duration of this event, the TMPA RT data not only significantly underestimated the peak intensities observed in the Zhouqu storm, the short downpour obviously could not suffice for an extreme daily or even-longer rain event. The 1-day ARI for the Zhouqu, China case does show a slightly increased ARI near the landslide site; however, the ARI values and maximum precipitation for this event are both fairly low. This case indicates that a sub-daily observing window may be necessary for this type of short event. The same issues may also apply to the Brazil 2011 landslide event (Case 2), where an estimated 250 mm of rain fell within 24 h, corresponding to a maximum ARI of 52 years for the 1-day window in the mountainous areas of Teresópolis and Nova Friburgo northwest of Rio De Janeiro (Phillips, 2011). However, a less significant ARI was reported in the 3-day and 5-day windows. These cases illustrate the importance of near-real-time, high quality and high-resolution rainfall estimates for predicting the potential landslides.

4. Discussion

The GLC provides an opportunity to characterize differences in landslide occurrence by time, geography, and impacts. While landslides are controlled by the complex interaction of multiple climatic and

Table 4

Results for five test cases resulting in significant landslide events within the GLC catalog. Top section displays the event information including the location, date, trigger and number of fatalities. The middle section displays the rainfall average recurrent interval (ARI) in years for rainfall within a $5 \times 5^\circ$ box centered on the landslide location. The maximum ARI was computed for 1–10 days and results are shown here for the 1, 3, and 7-day accumulations. The bottom section displays the accumulated rainfall at the GLC point (in mm) for the same 1, 3, and 7-day thresholds.

		Case 1	Case 2	Case 3	Case 4	Case 5
Event information	Location	Shiaolin, Taiwan	Teresópolis, Brazil	Kedarnath, India	La Pintada, Mexico	Zhouqu, China
	Date	8/10/2009	1/12/2011	6/16/2013	9/16/2013	8/7/2010
	Trigger	Typhoon Morakot	Heavy rainfall	Heavy rainfall	Tropical Cyclone Manuel	Heavy rainfall
	Fatalities	491	424	5000	68	1765
ARI over $5 \times 5^\circ$ grid	Maximum ARI	190 years (5-day)	188 years (2-day)	77 years (7-day)	99 years (3-day)	8.5 years (1-day)
	1-day	Null	52.8	18.5	42.1	8.5
	3-day	4.1	18.3	9.8	99.1	2.6
	7-day	65.9	10.2	77.4	80.9	0.8
Rain accum. at GLC point	1-day	232.6	60.9	119.9	85.5	35.9
	3-day	454.1	128.1	300.6	180.9	35.9
	7-day	549.3	196.4	515.0	268.2	130.7

geomorphologic variables, the impacts of these hazards depend on where the events occur. Many studies have evaluated how the level of development of a country or region affects how disaster impacts are felt, either economically or in terms of fatalities. In a study evaluating a range of different natural disasters, *Cavallo and Noy (2010)* found that “the overwhelming majority of people affected and killed by natural disasters reside in developing countries.” The study found that the median incidence of fatalities from disasters in the most developed areas in Western Europe and North America is less than 0.1 person per million inhabitants compared to over 1 person in Africa or Latin America and the Caribbean. Comparisons of fatalities by country and region in Fig. 4 and by GDP in Fig. 5 generally support these findings.

The length and size of the GLC enable more detailed comparisons of landslide triggering conditions across the globe. We consider extreme rainfall accumulations of only 1 to 10 days surrounding the reported landslide event. However, antecedent rainfall may have caused pore

pressures to increase in the landslide initiation zones and therefore, only a small rainfall event may have been needed to cause instability. While we do not account for antecedent conditions in the current analysis, future work will involve considering how seasonal precipitation may impact the trends observed in the GLC. Other triggers may have contributed to increased instability (e.g. construction, development, deforestation, recent burned areas), and as a result, less (or no) rainfall may have been needed to cause a landslide.

Uncertainties in the present estimates may also arise from limitations of the current TMPA sampling capabilities and algorithm for certain precipitation scenarios. TRMM is a low-orbiting, non-sun-synchronous satellite that takes “snapshots” of precipitation as it passes over a region. As a result, the instruments may miss the peak intensity of a short but intense thunderstorm—or miss the storm altogether. Rainfall in complex topography is also difficult to estimate due to complicated temperature characteristics of the clouds and interference with

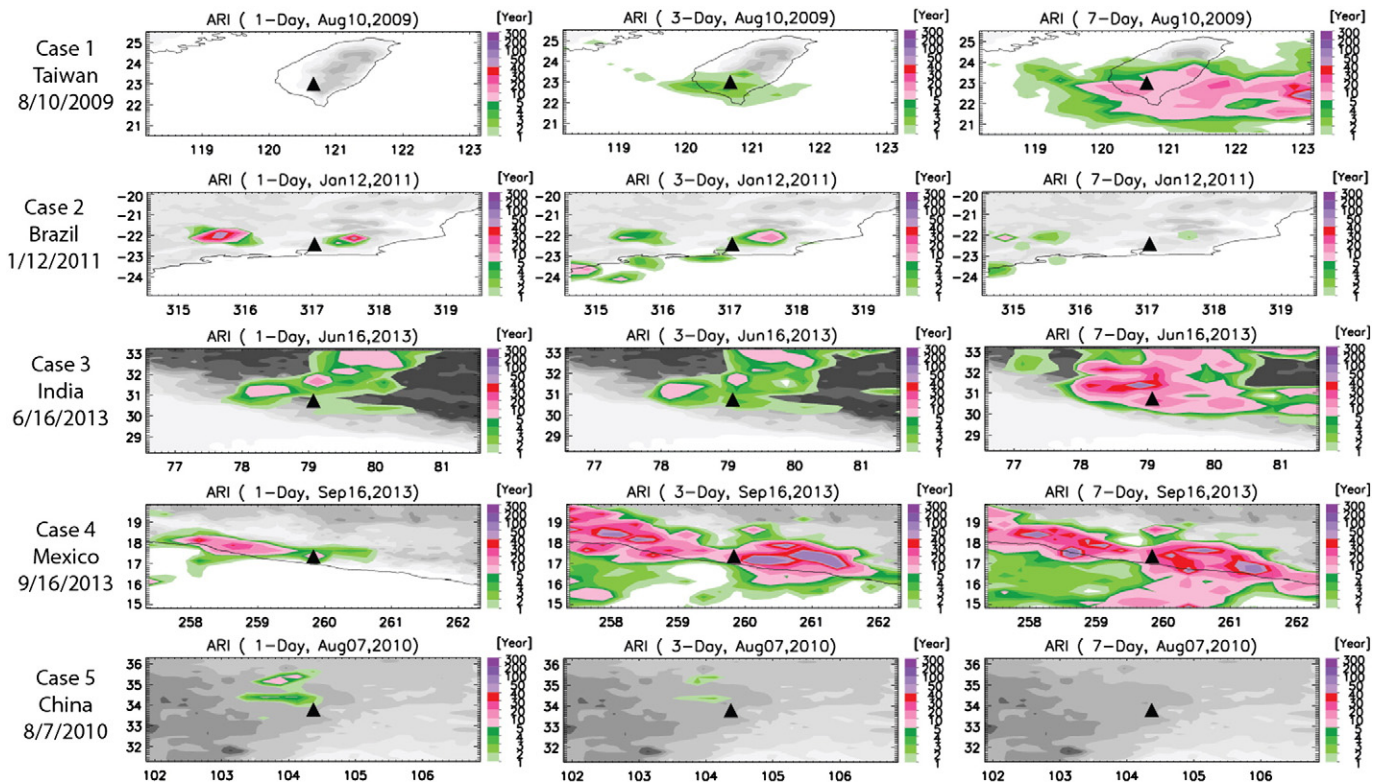


Fig. 9. Results of average recurrence interval (ARI) results for five extreme landslides in the GLC. Plots show the landslide location (black triangle) centered in a $5 \times 5^\circ$ box. ARI is calculated for 1, 3 and 7-day (left, center and right columns, respectively) rain accumulations prior to the landslide event for each of the 5 cases.

background terrain (Vicente et al., 2002; Adam et al., 2006). Lastly, many of the GLC events occur along coastlines or over small islands, such as much of the Philippines and Indonesia. The current resolution of the TMPA RT database is $0.25 \times 0.25^\circ$, which tends to mask out local precipitation features for smaller islands and coastlines. The TMPA algorithm also has artifacts associated with coastal regions that are sensor and scene-dependent, which can result in unsatisfactory precipitation estimates in certain situations (Huffman and Bolvin, 2012). The Global Precipitation Measurement (GPM; www.nasa.gov/gpm) mission, which was launched in February 2014, builds upon the TRMM methodology and will provide a more accurate global picture of precipitation at a $0.1 \times 0.1^\circ$, 30 minute resolution. The higher spatio-temporal resolution and accuracy should improve upon our current ability to identify small, intense precipitation features that frequently trigger landslides.

While satellite estimates of rainfall have some limitations in resolving specific rainfall features (shallow orographic events and short-duration, high-intensity events), the continuous multi-year record available from TMPA provides a unique way to evaluate how landslide activity relates to extreme rainfall. These types of integrated analyses can provide the foundation for establishing landslide-triggering rainfall thresholds at the local, regional or global scale. Both the percentile and ARI methods can be deployed to run in real-time and continuously evaluate the potential for new landslide events.

5. Conclusions

This paper outlines the methodology used to create a global landslide catalog based on media reports, online databases, and other sources. The 5741 points in the GLC provide a foundation for evaluating spatial and temporal trends in landslide activity from 2007 to 2013. Due to the biases intrinsic to this type of data collection, we observe patterns of landslide reporting related to urbanization and development, as well as to the prevalence of English-language media in some regions (North America, Europe) relative to others (South America, Asia). In spite of these biases, the GLC can be used for a variety of applications to understand both patterns of landslide occurrence and the relationship with extreme rainfall.

Further hazard modeling studies may help to better characterize biases including those related to population and road network densities by identifying a background hazard database of potential landslide activity independent from the GLC. Additional geomorphologic variables including topography, soil type, geology, distance to drainage areas, etc. are key indicators of potential landslide activity at the global scale. Ongoing work is focused on applying the GLC with other available inventories at the regional level to better characterize the geomorphologic variables most critical to computing landslide susceptibility. With additional years of data and improved accuracy in reporting, the GLC can provide a key database for improving the global picture of landslide susceptibility.

Evaluation of the GLC with the TMPA satellite-based archive demonstrates a clear relationship between a majority of the GLC points and extreme rainfall (greater than the 90th percentile or ARI greater than 5–10 years). Results also show that the GLC can be used to refine existing ID thresholds or define new extreme rainfall thresholds, which could potentially be used as guides to locate areas where landslides have been underreported. While the precipitation analysis results indicate that extreme landslide-triggering rainfall may be better resolved with shorter duration windows such as a daily threshold, it may also be likely that the sampling of precipitation at even the 1-day accumulation window may be too long for rainfall-triggering events that take place over several hours, such as in climates with strong diurnal rainfall patterns. While there are limitations to existing satellite-based precipitation estimates, new products from missions like GPM may improve the global representation of extreme rainfall and improve our understanding of landslide dynamics.

Acknowledgments

The authors acknowledge the individuals who helped to develop the GLC, including Stephanie Hill, Lynne Shupp, Teddy Allen, Pradeep Adhikari, Lauren Redmond, David Adler, Kimberly Rodgers, Lee Sanders, Benjamin Hall, and Melanie Franchek. This work was supported by the NASA SERVIR program (NNH11ZDA001N-SERVIR) and the Global Precipitation Measurement (GPM) mission. Thanks also to Yudong Tian, who helped provide the TMPA data for this analysis.

References

- Adam, J.C., Clark, E.A., Lettenmaier, D.P., 2006. Correction of global precipitation products for orographic effects. *J. Clim.* 19, 15–38.
- Berman, M., 2014. Everything you need to know about the Washington landslide. *Washington Post* (<http://www.washingtonpost.com/news/post-nation/wp/2014/03/24/everything-you-need-to-know-about-the-washington-landslide/>).
- Bonnin, G.M., Todd, D., Lin, B., Parzybok, T., Yekta, M., Riley, D., 2003. *Rainfall-frequency atlas of the United States*. NOAA Atlas 14 Volume 1. National Weather Service, Silver Spring, Maryland.
- Booth, A.M., Roering, J.J., Perron, J.T., 2009. Automated landslide mapping using spectral analysis and high-resolution topographic data: Puget Sound lowlands, Washington, and Portland Hills, Oregon. *Geomorphology* 109, 132–147. <http://dx.doi.org/10.1016/j.geomorph.2009.02.027>.
- Bright, E.A., Coleman, P.R., Rose, A.N., Urban, M.L., 2012. LandScan 201. LandScan (<http://www.ornl.gov/landscan/>).
- Bucknam, R.C., Coe, J.A., Chavarria, M.M., Godt, J.W., Tarr, A.C., Bradley, L., Rafferty, S., Hancock, D., Dart, R.L., Johnson, M.L., 2001. Landslides triggered by Hurricane Mitch in Guatemala – inventory and discussion. *U.S. Geol. Surv. Open-File Rep.* 01-443, pp. 1–40.
- Caine, N., 1980. The rainfall intensity: duration control of shallow landslides and debris flows. *Geogr. Ann. Phys. Geogr.* 62, 23–27.
- Cavallo, E., Noy, I., 2010. The economics of natural disasters – a survey. IDB Working Paper Series No. IDB-WP-124 (<http://www.iadb.org/res/publications/pubfiles/pubidb-wp-124.pdf>).
- Crosta, G.B., Frattini, P., 2001. Rainfall thresholds for triggering soil slips and debris flow. In: Mugnai, A., Guzzetti, F., Roth, A. (Eds.), *Mediterranean Storms Publ. GNDCI n. 2547*, Siena, Italy, pp. 463–487.
- Crozier, M.J., 1999. Prediction of rainfall-triggered landslides: a test of the antecedent water status model. *Earth Surf. Process. Landf.* 24, 825–833.
- Cruden, D., Varnes, D., 1996. Landslide types and processes. In: Turner, A., Shuster, R. (Eds.), *Landslides: investigation and mitigation*. Transp Res Board, Spec Rep 247, pp. 36–75.
- ESRI, 2011. ArcGIS Desktop: Release 10. URL: <http://www.esri.com>.
- Frattini, P., Crosta, G., Sosio, R., 2009. Approaches for defining thresholds and return periods for rainfall-triggered shallow landslides. *Hydrol. Process.* 1460, 1444–1460.
- Guha-Sapir, D., Below, R., Hoyois, P., 2014. International Disaster Database, Univ. Cathol. Louvain - Brussels - Belgium, EM-DAT www.em-dat.net (Accessed 20 March 2014).
- Guzzetti, F., 2000. Landslide fatalities and evaluation of landslide risk in Italy. *Eng. Geol.* 58, 89–107.
- Guzzetti, F., Cardinali, M., Reichenbach, P., 1994. The AVI project: a bibliographical and archive inventory of landslides and floods. *Environ. Manag.* 18, 623–633.
- Guzzetti, F., Mondini, A.C., Cardinali, M., Fiorucci, F., Santangelo, M., Chang, K.-T., 2012. Landslide inventory maps: new tools for an old problem. *Earth Sci. Rev.* 112, 42–66. <http://dx.doi.org/10.1016/j.earscirev.2012.02.001>.
- Guzzetti, F., Peruccacci, S., Rossi, M., Stark, C.P., 2008. The rainfall intensity–duration control of shallow landslides and debris flows: an update. *Landslides* 5, 3–17. <http://dx.doi.org/10.1007/s10346-007-0112-1>.
- Haigh, M.J., Rawat, J.S., Rawat, M.S., Bartarya, S.K., Rai, S.P., 1995. Interactions between forest and landslide activity along new highways in the Kumaun Himalaya. *For. Ecol. Manag.* 78, 173–189.
- Hong, Y., Adler, R., Huffman, G., 2006. Evaluation of the potential of NASA multi-satellite precipitation analysis in global landslide hazard assessment. *Geophys. Res. Lett.* 33, 1–5. <http://dx.doi.org/10.1029/2006GL028010>.
- Huffman, G.J., Adler, R.F., Bolvin, D.T., Gu, G., Nelkin, E.J., Bowman, K.P., Hong, Y., Stocker, E.F., Wolff, D.B., 2007. The TRMM multisatellite precipitation analysis (TMPA): quasi-global, multiyear, combined-sensor precipitation estimates at fine scales. *J. Hydrometeorol.* 8, 38–55. <http://dx.doi.org/10.1175/JHM560.1>.
- Huffman, G.J., Adler, R.F., Bolvin, D.T., Nelkin, E.J., 2010. The TRMM multi-satellite precipitation analysis (TMPA). In: Hossain, F., Gebremichael, M. (Eds.), *Satellite Rainfall Applications for Surface Hydrology*. Springer Verlag, pp. 3–22.
- Huffman, G.J., Bolvin, D.T., 2012. Real-Time TRMM Multi-Satellite Precipitation Analysis Data Set Documentation. (ftp://trmmopen.gsfc.nasa.gov/pub/merged/V7Documents/3B4XRT_doc_V7.pdf).
- Kirschbaum, D.B., Adler, R., Adler, D., Peters-Lidard, C., Huffman, G., 2012. Global distribution of extreme precipitation and high-impact landslides in 2010 relative to previous years. *J. Hydrometeorol.* 13, 1536–1551. <http://dx.doi.org/10.1175/JHM-D-12-02.1>.
- Kirschbaum, D.B., Adler, R., Hong, Y., Hill, S., Lerner-Lam, A., 2010. A global landslide catalog for hazard applications: method, results, and limitations. *Nat. Hazards* 52, 561–575. <http://dx.doi.org/10.1007/s11069-009-9401-4>.

- Kirschbaum, D.B., Adler, R., Hong, Y., Lerner-Lam, A., 2009. Evaluation of a preliminary satellite-based landslide hazard algorithm using global landslide inventories. *Nat. Hazards Earth Syst. Sci.* 9, 673–686.
- Larsen, M.C., Parks, J.E., 1997. How wide is a road? The association of roads and mass-wasting in a forested montane environment. *Earth Surf. Process. Landf.* 22, 835–848.
- Larsen, M.C., Simon, A., 1993. A rainfall intensity–duration threshold for landslides in a humid-tropical environment, Puerto Rico. *Geogr. Ann. Phys. Geogr.* 75, 13–23.
- Meyer, N.K., Dyrddal, A.V., Frauenfelder, R., Ertel Müller, B., Nadim, F., 2012. Hydrometeorological threshold conditions for debris flow initiation in Norway. *Nat. Hazards Earth Syst. Sci.* 12, 3059–3073. <http://dx.doi.org/10.5194/nhess-12-3059-2012>.
- Murillo-García, F., Alcántara-Ayala, I., Ardizzone, F., Cardinali, M., Fiorucci, F., Guzzetti, F., 2014. Satellite stereoscopic pair images of very high resolution: a step forward for the development of landslide inventories. *Landslides* 1–15. <http://dx.doi.org/10.1007/s10346-014-0473-1>.
- Oster, S., McMahon, D., 10 Aug 2010. Mudslide toll rises as Beijing mobilizes. *Wall Street J.* (<http://online.wsj.com/news/articles/SB10001424052748703435104575421170100705034>).
- Petley, D., 2012. Global patterns of loss of life from landslides. *Geology* G33217, 1–4. <http://dx.doi.org/10.1130/G33217.1>.
- Petley, D.N., Dunning, S.A., Rosser, N.J., 2005. The analysis of global landslide risk through the creation of a database of worldwide landslide fatalities. In: Hungr, O., Fell, R., Counture, R., Ebergardt, E. (Eds.), *Landslide Risk Management*. Balkema, Amsterdam, pp. 367–374.
- Petley, D.N., Hearn, G.J., Hart, A., Rosser, N.J., Dunning, S.A., Owen, K., Mitchell, W.A., 2007. Trends in landslide occurrence in Nepal. *Nat. Hazards* 43, 23–44. <http://dx.doi.org/10.1007/s10669-006-9100-3>.
- Phillips, T., 2011. Brazil landslides leave hundreds of people dead. *The Guardian* (<http://www.theguardian.com/world/2011/jan/12/brazil-landslide-leaves-115-dead>).
- Pradhan, B., 2010. Remote sensing and GIS-based landslide hazard analysis and cross-validation using multivariate logistic regression model on three test areas in Malaysia. *Adv. Space Res.* 45, 1244–1256. <http://dx.doi.org/10.1016/j.asr.2010.01.006>.
- Snohomish, 2014. Snohomish County, Medical Examiner's Office Media Update: May 27, 2014 regarding the Oso, Washington mudslide (Everett, Washington).
- USGS, 2004. Landslide Types and Processes. Facts Sheet 2004-3072 1–4. (<http://pubs.usgs.gov/fs/2004/3072/>).
- Vicente, G.A., Davenport, J.C., Scofield, R.A., 2002. The role of orographic and parallax corrections on real time high resolution satellite rainfall rate distribution. *Int. J. Remote Sens.* 23, 221–230. <http://dx.doi.org/10.1080/01431160010006935>.
- Vmap0, 2009. National Imagery and Mapping Agency: Vector Map Level 0 (VMap). <http://earth-info.nga.mil/publications/vmap0.html>.
- World Bank, 2014. GDP per capita (current US\$). World Bank (<http://data.worldbank.org/indicator/NY.GDP.PCAP.CD>).
- Xu, C., Xu, X., Yao, X., Dai, F., 2013. Three (nearly) complete inventories of landslides triggered by the May 12, 2008 Wenchuan Mw 7.9 earthquake of China and their spatial distribution statistical analysis. *Landslides* 1–21. <http://dx.doi.org/10.1007/s10346-013-0404-6>.
- Zhou, Y., Lau, K.M., Huffman, G., 2015. Mapping TRMM TMPA into average recurrence interval for monitoring extreme precipitation events. *J. Appl. Meteorol Climatol* <http://dx.doi.org/10.1175/JAMC-D-14-0269.1> (in press).